Acta Crystallographica Section D
Biological Crystallography
ISSN 0907-4449

Structure analysis of *Entamoeba histolytica* enolase

Eike C. Schulz,[a]* Michael Tietzel,[a] Ayala Tovy,[b] Serge Ankri[b] and Ralf Ficner[a]

[a]Abteilung für Molekulare Strukturbiologie, Institut für Mikrobiologie und Genetik, Georg-August-Universität Göttingen, Justus-von-Liebig Weg 11, 37077 Göttingen, Germany, and [b]Faculty of Medicine, Rappaport Institute, Technion – Israel Institute of Technology, Israel

Correspondence e-mail: eschulz1@gwdg.de

Received 5 March 2011
Accepted 2 May 2011

PDB Reference: *E. histolytica* enolase, 3qtp.

Entamoeba histolytica enolase (EhENO) reversibly interconverts 2-phosphoglyceric acid (2-PGA) and phosphoenolpyruvic acid (PEP). The crystal structure of the homodimeric EhENO is presented at a resolution of 1.9 Å. In the crystal structure EhENO presents as an asymmetric dimer with one active site in the open conformation and the other active site in the closed conformation. Interestingly, both active sites contain a copurified 2-PGA molecule. While the 2-PGA molecule in the closed active site closely resembles the conformation known from other enolase–2-PGA complexes, the conformation in the open active site is different. Here, 2-PGA is shifted approximately 1.6 Å away from metal ion I, most likely representing a precatalytic situation.

1. Introduction

Entamoeba histolytica is a globally distributed gastrointestinal protozoan parasite and the causative agent of amoebiasis in humans. *E. histolytica* causes 50 million infections annually, of which 100 000 develop fatally; a higher mortality rate is only observed for malaria among protozoan infections (Baxt & Singh, 2008; World Health Organization, 1997). Reports of *in vitro* resistance towards the standard therapeutic metronidazole and its undesirable side effects demand the examination of putative novel drug targets for the future treatment of *E. histolytica* amoebiasis (Petri, 2003; Samarawickrema *et al.*, 1997; Tally *et al.*, 1975). Since *E. histolytica* lacks mitochondria, its ATP production is only maintained by the glycolytic pathway (McLaughlin & Aley, 1985; Reeves, 1984; Rosenbaum & Wittner, 1970). As a consequence, glycolytic enzymes might be suitable drug targets for effective amoebiasis therapy. A well studied example of a glycolytic enzyme is enolase (2-phospho-D-glycerate hydrolase; EC 4.2.1.11). During glycolysis and gluconeogenesis, enolase catalyses the reversible interconversion of 2-phosphoglyceric acid (2-PGA) and phosphoenolpyruvic acid (PEP). Enolase is a highly conserved metal-activated metalloenzyme that consists of a smaller N-terminal domain and a larger C-terminal domain. In eukaryotes, enolase typically assembles into homodimers (Brewer, 1981; Lebioda & Stec, 1988; Lebioda *et al.*, 1989; Reed *et al.*, 1996). Several crystal structures of enolase show that the N-terminal α/β-domain consists of a three-stranded antiparallel β-sheet and four α-helices, while the C-terminal domain displays an unusual eightfold α/β-barrel. This α/β-

Table 1
Data-collection and refinement statistics.

Values in parentheses are for the highest resolution shell.

Data collection	
Wavelength (Å)	0.9181
Unit-cell parameters	
a (Å)	64.42
b (Å)	92.62
c (Å)	160.58
α (°)	90.0
β (°)	90.0
γ (°)	90.0
Space group	$P2_12_12_1$
Resolution range (Å)	46.34–1.90 (2.00–1.90)
No. of reflections	278074 (35952)
Average $I/\sigma(I)$	12.75 (3.38)
Completeness (%)	98.8 (92.9)
Multiplicity	3.6 (3.6)
$R_{\rm meas}$ (%)	11.0 (47.1)
Refinement	
Resolution limits (Å)	46.31–1.90 (1.92–1.90)
No. of used reflections	75583 (2440)
No. of protein atoms	6769
No. of ligand atoms	54
No. of water atoms	1118
R factor (%)	15.29 (23.40)
$R_{\rm free}$ (%)	20.17 (31.28)
Ramachandran plot statistics	
Most favourable region (%)	97.5
Generously allowed regions (%)	2.3
Disallowed regions (%)	0.2
R.m.s. deviations from ideal values	
Bond distances (Å)	0.007
Angles (°)	1.013

barrel differs from typical triose-phosphate isomerase (TIM) barrels by exhibiting a $\beta_2\alpha_2(\beta\alpha)_6$ topology (Chai *et al.*, 2004; da Silva Giotto *et al.*, 2003; Duquerroy *et al.*, 1995; Hosaka *et al.*, 2003; Kang *et al.*, 2008; Kühnel & Luisi, 2001; Lebioda & Stec, 1988; Lebioda *et al.*, 1989; Stec & Lebioda, 1990). The highly conserved active site is situated in the C-terminal domain, in which the β-elimination reaction is catalysed using the ε-amino group of a lysine residue (Lys345 in yeast) and the acidic side chain of a glutamic acid residue (Glu211 in yeast) for general base and general acid catalysis, respectively (Reed *et al.*, 1996). The activity of enolase also depends on the presence of certain divalent metal ions, naturally magnesium (Brewer, 1981). One of the divalent metal ions (metal I) is coordinated by three carboxyl side chains within the active site and binds the carboxyl group of the substrate/product (Larsen *et al.*, 1996; Wedekind *et al.*, 1995). However, catalysis is not only carried out by residues from the C-terminal domain but also depends on the closure of a loop from the N-terminal domain (residues 37–43 in yeast; L1). This loop contains a serine residue that together with a phosphoryl O atom of the substrate/product chelates another divalent metal ion in the active site (metal II; Larsen *et al.*, 1996; Reed *et al.*, 1996; Wedekind *et al.*, 1994). In addition to the 'open' and 'closed' conformations induced by the closure of L1 over the active site, a third 'semiclosed' conformation has been observed in yeast enolase. In the 'semiclosed' conformation the loop containing His157 (residues 153–166 in yeast; L2) is shifted by 3.5 Å in comparison to the fully closed conformation and lacks direct interaction with the substrate; instead, it forms a hydrogen bond to a water molecule (Larsen *et al.*, 1996; Zhang *et al.*, 1997). However, in addition to its function in glycolysis, enolase has also been reported to play roles in various diseases (Kim & Dang, 2005; Pancholi, 2001), in transcriptional regulation (Chang *et al.*, 2003; Feo *et al.*, 2000; Kim & Dang, 2005; Subramanian & Miller, 2000), as a heat-shock protein (Iida & Yahara, 1985), as the τ-crystallin in the turtle eye lens (Wistow & Piatigorsky, 1987) and in the RNA degradosome (Kühnel & Luisi, 2001; Nurmohamed *et al.*, 2010; Py *et al.*, 1996), and to be expressed on cell surfaces as a plasminogen-binding receptor (Miles *et al.*, 1991). Additionally, it has been shown that enolase exhibits fibronectin-binding properties (Castaldo *et al.*, 2009; Esgleas *et al.*, 2008). Within *Entamoeba* species, enolase has been reported to be involved in the encystation process (*E. invadens*; Segovia-Gamboa *et al.*, 2010) and has also been implicated in metabolic regulation of the (cytosine-5)-methyltransferase 2 (Dnmt2) EhMeth (*E. histolytica*; Tovy *et al.*, 2010).

Here, the crystal structure of enolase from *E. histolytica* (EhENO) is presented at a resolution of 1.9 Å. The crystal structure shows an asymmetric homodimeric enzyme with one active site in the open conformation and one active site in the closed conformation. Interestingly, both active sites contain a copurified substrate molecule.

2. Methods

2.1. Protein purification and crystallization

The gene for *E. histolytica* enolase (XP_649161.1) was cloned from genomic DNA into the pGEX6-P3 vector (GE Healthcare); protein expression was conducted in *Escherichia coli* BL21 (DE3) in TB medium at 289 K for 18 h. The GST-fusion protein was purified using GSH Sepharose (100 m*M* Tris–HCl pH 7.5, 250 m*M* NaCl, 5 m*M* $MgCl_2$, 1 m*M* dithiothreitol) following the manufacturer's instructions. Subsequently, the eluate was incubated with PreScission protease [1:100(*w*:*w*); GE Healthcare] for 18 h at 277 K. In order to remove glutathione, the buffer was exchanged using a desalting column (100 m*M* Tris–HCl pH 7.5, 250 m*M* NaCl, 5 m*M* $MgCl_2$, 1 m*M* dithiothreitol) and cleaved GST as well as uncleaved fusion protein were removed by a second GSH Sepharose purification step. The homodimeric EhENO was further purified by Superdex S-75 size-exclusion chromatography (100 m*M* Tris–HCl pH 7.5, 100 m*M* NaCl, 5 m*M* $MgCl_2$). Purified enolase was concentrated to 7.5 mg ml^{-1} and stored at 193 K until further use. Protein concentration was determined using the Bradford assay. Crystals were grown at 293 K in sitting-drop vapour-diffusion plates, combining equal volumes of precipitant [100 m*M* Bis-Tris pH 5.5, 25%(*w*/*v*) PEG 3350, 200 m*M* ammonium sulfate] and protein solution. Crystals were cryoprotected by soaking them in precipitant solution containing an additional 12%(*v*/*v*) 2,3-butanediol and were flash-frozen in liquid nitrogen prior to data collection.

2.2. Data collection and processing

X-ray data collection was performed at 100 K; diffraction images were collected on beamline 14.1 at BESSY, Berlin. Diffraction images were indexed, integrated and scaled using *XDS* and *XSCALE*, respectively (Kabsch, 2010*a*,*b*).

2.3. Molecular replacement and structure refinement

The structure was solved by molecular replacement (*Phaser*; McCoy *et al.*, 2007) using the *E. coli* enolase structure (PDB entry 1e9i; Kühnel & Luisi, 2001) as a search model. Model building was performed in *Coot* (Emsley *et al.*, 2010). Coordinates were refined to reasonable stereochemistry at a resolution of 1.9 Å using *PHENIX* (Adams *et al.*, 2010; Table 1). Alternating steps of refinement and structure adjustment were performed until the *R* values converged. The structure was validated using *MolProbity* (Chen *et al.*, 2010). Simulated-annealing OMIT maps were calculated in *CNS* (Brünger *et al.*, 1998).

2.4. Structure and sequence comparison

Calculation of r.m.s.d.s was performed with the program *LSQMAN* (Kleywegt, 1996). The brute-force function was applied with a fragment length of 30 residues, a fragment step size of one residue and a minimum of 200 matched residues. A distance cutoff of 3.5 Å was applied in all brute-force alignments. Comparison of the L1 conformation in various structures was performed using the Needleman–Wunsch alignment algorithm and r.m.s.d.s were calculated with the improve function, applying a distance cutoff of 15 Å. Sequence-identity calculations were performed using *LALIGN* (W. Pearson; http://www.ch.embnet.org/software/LALIGN_form.html).

2.5. Molecular visualization

All molecular images were generated in *PyMOL* (DeLano, 2002).

3. Results

3.1. Overall structure

EhENO crystallized under multiple conditions; however, the best crystals were derived from conditions containing PEG and ammonium sulfate. These enolase crystals belonged to space group $P2_12_12_1$ and contained two monomers per asymmetric unit assembled into one homodimer. The structure was solved by molecular replacement using the structure of *E. coli* enolase as a search model. The structure could be refined at a resolution of 1.9 Å, giving rise to electron density of reasonable quality (Table 1). All 436 residues are visible in both molecules. Additionally, one and two residues resulting from cloning artefacts are visible at the N-terminal ends of chains *A* and *B*, respectively. With the exception of Arg404, all residues lie within allowed Ramachandran regions. The unfavourable conformation of Arg404 is held in position by an interaction of its main-chain amide with the carbonyl O atom of Ser14 of the same molecule. Additionally, its side chain forms contacts to the side chain of Glu406 and to the carbonyl O atom of Glu206, the latter of which belongs to a neighbouring molecule. After structure refinement, several tetrahedral difference map peaks could be observed in the electron density that resembled either phosphate or sulfate ions. Owing to the presence of sulfate in the crystallization condition, all of these peaks were modelled as sulfates.

Generally, each EhENO monomer can be separated into an N-terminal domain (residues 1–138) and a C-terminal domain (residues 139–436). The N-terminal domain consists of a three-stranded β-sheet packed against three α-helices, while an eightfold α/β-barrel constitutes the C-terminal domain and exhibits a $\beta_2\alpha_2(\beta\alpha)_6$ topology, which is typical of the enolase superfamily (Fig. 1*a*). Within the homodimeric EhENO the N-terminal domain of one chain packs against the C-terminal domain of the other chain, predominantly interacting by polar contacts. The two monomers can be superimposed with an r.m.s.d. of 0.43 Å calculated on C^α positions. However, despite this high similarity a large difference can be observed within the catalytically important loop 1 (L1; residues 37–43) between subunits *A* and *B*, with a deviation of up to 10 Å between compared C^α positions in the two subunits (Fig. 1*b*).

3.2. Subunit *A*: the open conformation

Subunit *A* is present in the so-called open conformation since L1-*A* faces away from the active site, which in consequence is left wide open. In the crystalline environment L1-*A* is packed against the N-terminal domain of a neighbouring EhENO dimer. However, the conformation of L1-*A* closely resembles that previously observed in enolase structures in the open conformation and hence is not a mere crystal-packing artefact. In order to support this finding, the r.m.s.d. for L1-*A* was calculated in comparison to other enolase structures. Upon superposition with the structure of yeast enolase in the open conformation (PDB entry 3enl; Stec & Lebioda, 1990) EhENO L1-*A* displays an r.m.s.d. of 0.9 Å, while the r.m.s.d. increases to 2.4 Å when compared with the closed conformation (PDB entry 1ebg; Wedekind *et al.*, 1994). Interestingly, a superposition of L2 (residues 153–169) with a semiclosed yeast enolase (PDB entry 2one; Zhang *et al.*, 1997) yields an r.m.s.d. of 0.6 Å calculated on C^α positions for the respective area. This indicates that in addition to the open conformation of L1, L2 of subunit *A* also adopts the semiclosed conformation.

After refinement of the protein structure, remaining electron density was clearly visible in the active site. At first, the difference map peaks were refined placing only a phosphate ion in the density peak contacting Arg376 and Ser377. However, after refinement difference map peaks remained that could be best explained by the presence of 2-PGA in the active site. Hence, in further refinement steps a 2-PGA molecule was included instead of the phosphate, albeit with a reduced occupancy (0.2) for all nonphosphate atoms (Fig. 2*a*). The presence of 2-PGA in the active site was further supported by calculation of a simulated-annealing OMIT map. The simulated-annealing OMIT map clearly shows electron density that strongly correlates with the presence of a 2-PGA

molecule that is bound by Gln164, Glu208, Lys347, Arg376 and Ser377 (Fig. 2*b*). Additionally, 2-PGA interacts with several water molecules. Furthermore, the carboxyl group of the 2-PGA molecule is involved in coordination of the conformational metal ion I. This metal ion is further coordinated by Asp243, Glu296, Asp322 and two water molecules in an octahedral manner. The nature of the metal ion could not be unambiguously determined from the metal–oxygen distances of between 2.4 and 2.5 Å. However, the metal–oxygen distances are within two standard deviations of the mean metal–oxygen distance described for Mg^{2+} ions (Dokmanić *et al.*, 2008). Hence, consistent with previous reports, the octahedral coordination sphere, the presence of Mg^{2+} during protein purification and the fact that Mg^{2+} is the natural ligand of enolase supported modelling of the difference density peak as an Mg^{2+} ion (Brewer, 1981; Duquerroy *et al.*, 1995; Larsen *et al.*, 1996; Lebioda *et al.*, 1989; Wedekind *et al.*, 1994, 1995).

3.3. Subunit *B*: the closed conformation

Subunit *B* is present in the closed conformation since L1-*B* firmly closes over the active site. However, in contrast to subunit *A*, L1-*B* is not in contact with other symmetry-related molecules forming the crystal lattice and the electron density

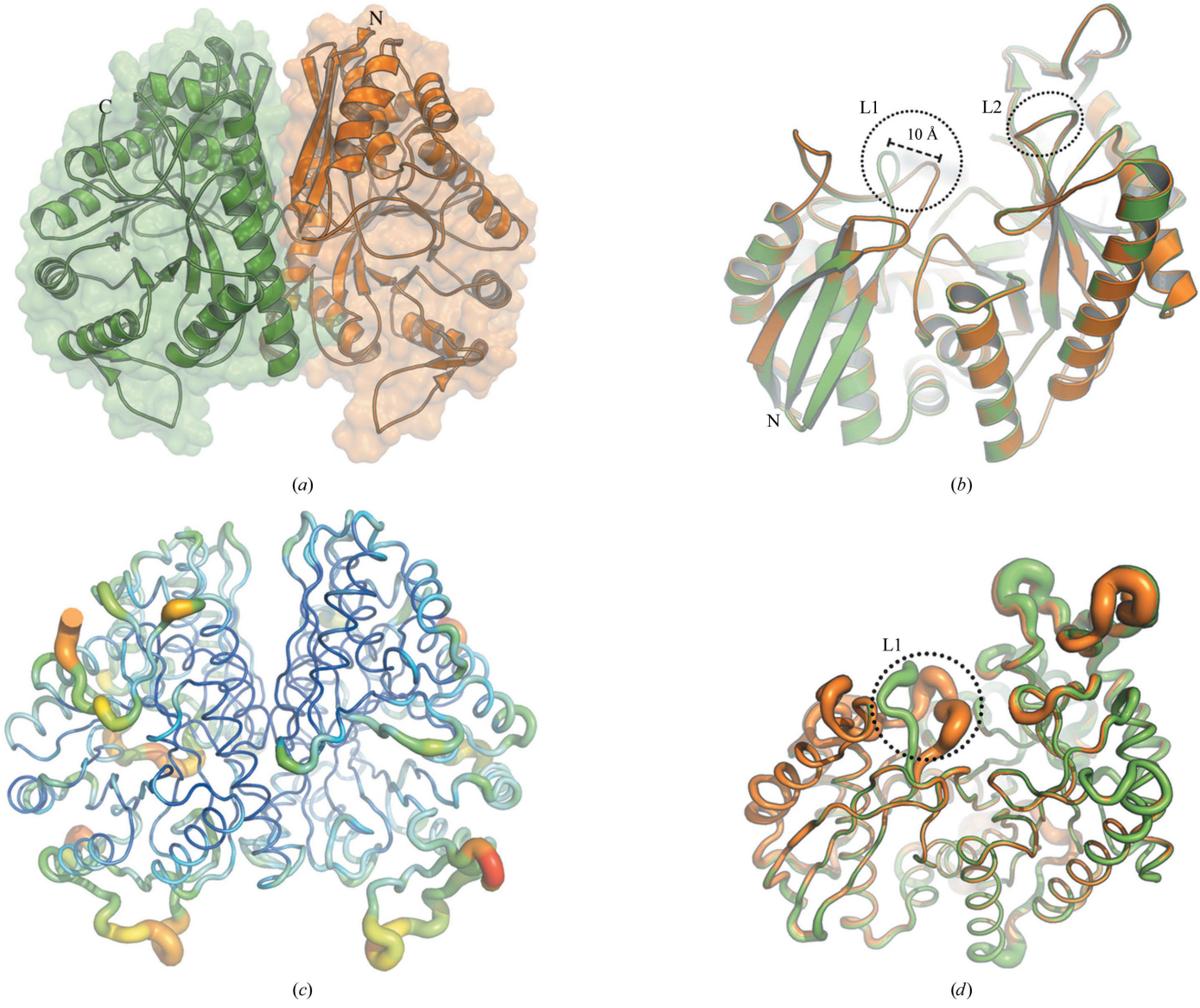

Figure 1
Crystal structure of *E. histolytica* enolase (EhENO). (*a*) EhENO is a highly conserved homodimeric enzyme. Secondary-structure elements and a semi-transparent surface are shown in green for subunit *A* and in orange for subunit *B*; the N-terminus of molecule *B* and the C-terminus of molecule *A* are indicated. (*b*) A superposition shows the high degree of similarity between the two subunits. However, within the catalytically important loop L1 the subunits differ by up to 10 Å. Virtually no difference can be observed in L2. (*c*) The figure is coloured according to *B* factor, where blue denotes a low *B* factor and red a high *B* factor. The tube thickness is also related to *B* factor: a thin tube indicates a low *B* factor and a thick tube indicates a high *B* factor. EhENO is a generally rigid molecule as indicated by the relatively low temperature factors. However, higher disorder can be observed within surface-exposed loop structures, presumably owing to increased flexibility in these areas. (*d*) A superposition of both subunits with tube thickness corresponding to *B* factor; a thicker tube indicates an increased *B* factor. Particular flexibility can be observed for L1 of subunit *B* (L1-*B*) that shields the active side.

for L1-*B* is less well defined. This indicates a higher flexibility, which is supported by increased *B* values in this area (Figs. 1*c* and 1*d*). Remaining stretches of difference density suggest that a minor fraction of subunit *B* is also present in the open conformation; however, the density for this putative alternate conformation was too weak to be properly modelled. In order to compare the conformation of L1-*B* with those of other enolase structures it was superposed with the structure of yeast enolase in the open conformation (PDB entry 3enl; Stec & Lebioda, 1990), showing an r.m.s.d. of 2.7 Å, which decreased to 0.5 Å when compared with the closed conformation (PDB entry 1ebg; Wedekind *et al.*, 1994). Similar to subunit *A*, a comparison of L2 (residues 153–169) with a semiclosed yeast enolase structure (PDB entry 2one; Zhang *et al.*, 1997) yielded an r.m.s.d. of 0.6 Å for the respective area, indicating that subunit *B* also adopts a semiclosed conformation.

In the active site of subunit *B* electron density clearly resembling a 2-PGA molecule was present, which was also supported by a simulated-annealing OMIT map (Figs. 2*c* and 2*d*). The 2-PGA molecule identified in subunit *B* closely resembles the conformation observed in other enolase molecules in the closed conformation. However, in comparison to the active site of subunit *A* the 2-PGA molecule is shifted by 1.3–1.9 Å towards the conformational metal ion I. Metal ion I is coordinated by Asp243, Glu296, Asp322, a water molecule and the carboxyl group of 2-PGA. 2-PGA itself is bound by

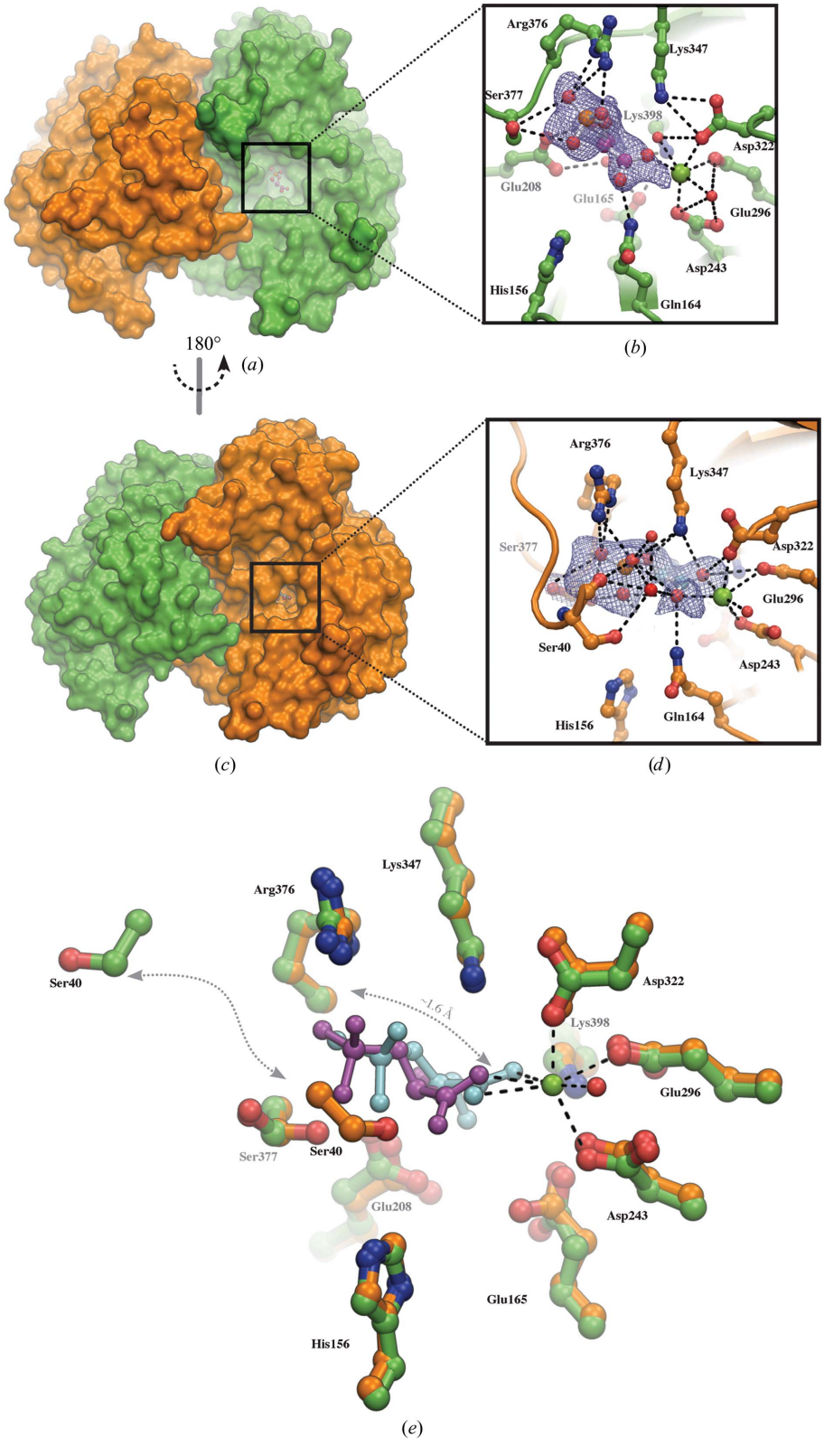

Figure 2
The active sites of both subunits contain a substrate molecule. (*a*) Surface representation of EhENO; the substrate molecule is visible in the active site of subunit *A* (green). (*b*) Close-up of the active site of subunit *A*: the 2-PGA molecule is shown as a ball-and-stick representation in purple and important residues are shown in a green stick representation. Metal ion I is depicted as a green sphere. The presence and conformation of 2-PGA is supported by an $|F_o - F_c|$ simulated-annealing OMIT map displayed at 2.5σ (blue mesh). (*c*) Surface representation of subunit *B* (orange); notably, 2-PGA is shielded by the closure of L1. (*d*) Close-up view of the active site of subunit *B*: the 2-PGA molecule is shown in a ball-and-stick representation in cyan and important residues are shown in an orange stick representation. Metal ions I and II are shown as green spheres. The presence and conformation of 2-PGA is supported by an $|F_o - F_c|$ simulated-annealing OMIT map displayed at 2.5σ (blue mesh). (*e*) A superposition of both EhENO active sites. With the exception of Ser40 all active-site residues overlap without major differences. Hence, the 1.3–1.9 Å displacement observed for 2-PGA from the open (purple) to closed (cyan) state must solely depend on the closure of L1 and the presence of the secondary metal ion.

Gln164, Glu165, Glu208, Lys347, Arg376, Ser377 and Lys398. The stretched density for the phosphate group of 2-PGA suggests that a second conformation of 2-PGA that is more reminiscent of the situation in active site *A* could also be bound in the active site. However, the density for this conformation was of overall poor quality, indicating a very low occupancy of the second conformation, which in consequence was not modelled.

In agreement with subunit *A*, a metal ion could be identified in subunit *B*. Again, an unambiguous determination of the metal ion was not possible, but for the same reasons as in subunit *A* it has been modelled as an Mg^{2+} ion. Typically, in closed conformations a second metal ion (metal II) can be found in the active site. However, difference map peaks that could correspond to a second metal ion were too distant (2.5–2.7 Å) from interacting atoms to be modelled as an Mg^{2+} ion and hence were interpreted as water molecules. These two water molecules bind to the phosphate group of the 2-PGA molecule and are further coordinated by the side-chain hydroxyl group and the main-chain carbonyl O atom of Ser40. This is in agreement with a structure of yeast enolase that is present in the closed conformation but also lacks the second metal ion (PDB entry 7enl; Lebioda & Stec, 1991).

4. Discussion

Like other enolases, EhENO is highly conserved, sharing high sequence identity with enolases from other organisms (Table 2). This sequence conservation also persists within the active site and the catalytic loops L1 (residues 37–43) and L2 (residues 153–166). However, there are also some mutations that suggest adaptation of EhENO to distinct environmental conditions. In contrast to all other enolase structures solved to date, EhENO displays a disulfide bond formed between Cys147 and Cys169 in each monomer despite the presence of 1 m*M* dithiothreitol during purification. The presence of a disulfide is interesting corresponding to the fact that intracellular disulfides are typically rare owing to the reducing environment of the cytosol. Interestingly, this area in enolases from other organisms is typically stabilized by hydrophobic interactions (Fig. 3, Figure S1[1]). However, the presence of disulfide bonds is not unique to EhENO, as other enzymes from *E. histolytica* have also been reported to contain disulfide bonds. *E. histolytica* UDP-glucose pyrophosphorylase has been suggested to be redox-regulated by the formation and cleavage of disulfide bonds (Martínez *et al.*, 2011). A similar regulation by the formation of disulfide bonds has also been described for *Giardia lamblia* triose-phosphate isomerase (GlTIM; Reyes-Vivas *et al.*, 2007). In these enzymes, the formation of disulfide bonds correlates with a reduction in enzymatic activity. However, a similar behaviour of EhENO has not yet been described. From a structural point of view, redox regulation of EhENO seems rather unlikely. Firstly, the disulfide bridge is situated in the core of the enzyme and does not hinder access to the active site, nor is it involved in the stabilization of a specific conformation that is required for catalysis. Secondly, the respective area in enolases from organisms that do not contain a disulfide bridge shows practically no difference from that of EhENO, suggesting that reduction of the disulfides will not lead to major structural changes (Fig. 3). This is supported by the partially reduced cysteines in chain *A* (Fig. 3*a*), which do not influence the conformation of the backbone. It can be speculated that the presence of a disulfide bond could lead to higher stability of the enzyme towards harsh conditions, which might provide an adaptation of *E. histolytica* to resist extra-intestinal environments. Furthermore, an extracellular role for EhENO is also conceivable. However, none of these roles has been described to date.

Table 2
Comparison of sequence identity of enolase structures to EhENO.

Organism	PDB code	Amino-acid identity (%)
Entamoeba histolytica	3qtp	100
Homo sapiens (neuron-specific)	1te6	63.8
Trypanosoma brucei	1oep	63.6
Homo sapiens	3b97	62.3
Hommarus gammarus	1pdy	61.3
Toxoplasma gondii	3otr	60.8
Saccharomyces cerevisiae	2one	59.2
Enterococcus hirae	1iyx	53.3
Streptococcus pneumoniae	1w6t	51.6
Escherichia coli	1e9i	51.2

As mentioned above, *E. histolytica* lacks mitochondria, therefore it depends solely on glycolysis for ATP production. This dependency bears potential in the design of species-specific enolase inhibitors. In the human pathogen *Trypanosoma brucei*, enolase is a validated drug target and EhENO shows high sequence similarity to this enzyme (Table 2; Figure S1; Navarro *et al.*, 2007). With respect to human enolase, the enolases from *T. brucei* and *E. histolytica* present a mutation at position 155 of L2 that has been suggested as a possible candidate for the design of species-specific enolase inhibitors. However, while position 155 is a lysine residue in *T. brucei* enolase, it is an alanine residue in EhENO. Opposite to Ala155, a surface-exposed lysine (Lys261) that is not conserved in human enolase can be found. Furthermore, another accessible cysteine (Cys409) can be found at the dimer interface of EhENO (Fig. 4). Commonly, these residues are either close to the catalytic centre or are surface-exposed. These features make them accessible to drugs and therefore specific inhibition or impairment of EhENO is not impossible. Encouragingly, partial inhibition of enolase activity has already been reported to be lethal to *T. brucei* (Albert *et al.*, 2005). With respect to the strict dependence on glycolysis, a similar effect is conceivable for *E. histolytica.* Certainly, the high sequence identity between human and amoebal enolases makes the design of species-specific drugs a challenging task and hence precise structural knowledge is an important prerequisite in order to proceed with any rational drug development. The suitability of EhENO for the design of

[1] Supplementary material has been deposited in the IUCr electronic archive (Reference: HV5185). Services for accessing this material are described at the back of the journal.

species-specific inhibitors has been discussed previously using a molecular-modelling approach (Hidalgo *et al.*, 1997). However, the lack of experimental data on the structure of EhENO prevented further steps, an obstacle which now has been overcome.

The stepwise catalysis of enolase depends on a kinetically well ordered sequence of binding events. Initially, metal I is coordinated, followed by binding of 2-PGA. In the next steps metal II binds to the phosphate group of 2-PGA and Ser40 (Ser39 in yeast) closes the active site (Poyner *et al.*, 2001, 2002; Reed *et al.*, 1996). Currently, the last step is structurally well described, with many structures that display enolase–substrate complexes in the closed conformation. In these complexes it has been established that the phosphate of 2-PGA is bound by an arginine and two serine residues, and the carboxyl function of 2-PGA is coordinated by an interaction with metal I, while the hydroxymethyl function of 2-PGA is in contact with a conserved glutamate (Larsen *et al.*, 1996; Reed *et al.*, 1996). Consistent with these previous findings, subunit *B* and the bound substrate of EhENO are present in the closed conformation. However, EhENO crystallized in the form of an asymmetric dimer that also bears an open active site. Asymmetric enolase dimers have been described previously and have typically been assigned to crystal-packing contacts which stabilize the distinct active-site conformations (Chai *et al.*, 2004; Sims *et al.*, 2006; Zhang *et al.*, 1997). A similar situation was also observed in EhENO, where crystal-packing contacts stabilize the open conformation of the active site of subunit *A*. However, only a few enolase structures in the open conformation have currently been described to contain a substrate molecule. The active sites of substrate-containing enolases in the open conformation display a remarkable similarity to each other that can also be found in L1, even though the proteins crystallized in different space groups (Fig. 5). However, despite this general active-site similarity either the active sites of these structures contain a phosphoglycolic acid (PGA) molecule that lacks the hydroxymethyl group or the 2-PGA substrate molecule has been modelled in a noncatalytic con-

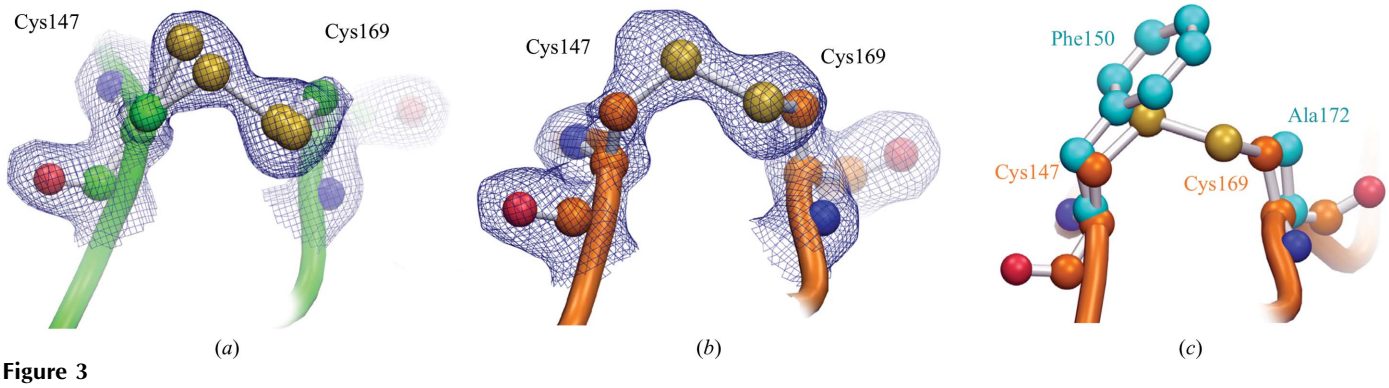

Figure 3
(*a*) The disulfide bridge within the EhENO monomers is formed between Cys147 and Cys169; in subunit *A* an alternate conformation (refined at 40% occupancy) with reduced cysteines is also visible. $2|F_o - F_c|$ density clearly showing the connection between the two residues is contoured at a level of 1.5σ. (*b*) As in (*a*) but for subunit *B*; no alternate conformation is visible. (*c*) In enolase structures from other organisms the same area is typically stabilized by hydrophobic interactions; this is illustrated by a superposition with yeast enolase (PDB entry 7enl; Lebioda & Stec, 1991), in which the structurally equivalent positions are occupied by Phe150 and Ala172 (cyan).

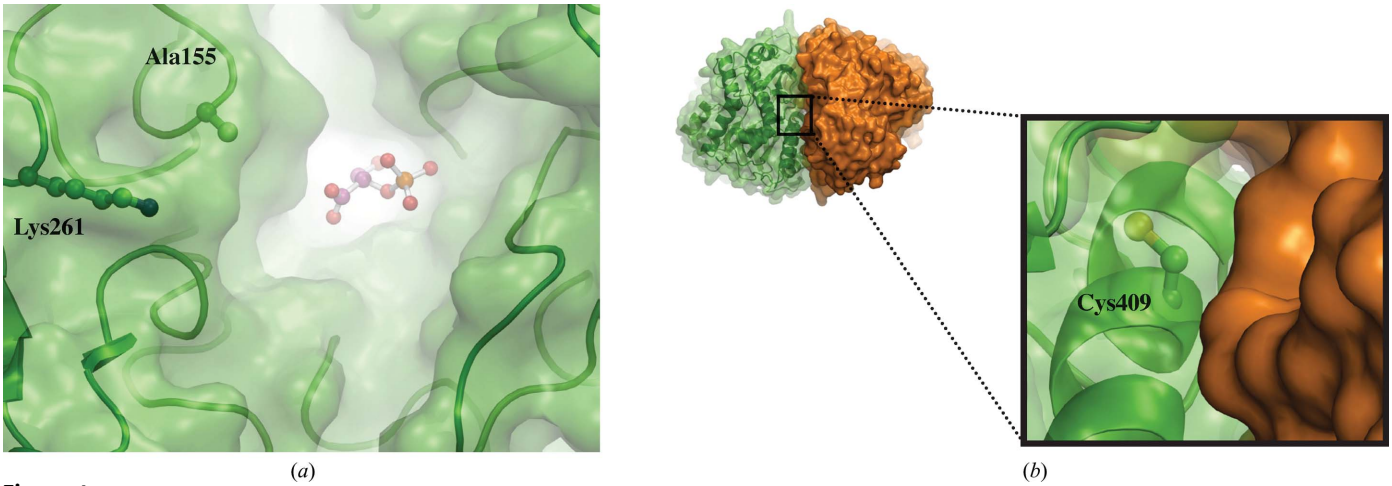

Figure 4
(*a*) Lys261 is exposed at the surface of EhENO and is situated at a distance of ∼15 Å from the catalytic centre (2-PGA is shown in ball-and-stick representation). In *T. brucei* residue 155 was suggested to be a potential candidate for the design of species-specific enolase inhibitors. (*b*) Cys409 situated at a distance of ∼15 Å from the active centre cannot be found in human enolase, but an alanine residue occupies the equivalent position. Cys409 is located at the dimer interface between subunit *A* and *B* and is a putative candidate residue for species-specific drug design.

formation probably limited by the available resolution (Fig. 5; Duquerroy *et al.*, 1995; Lebioda & Stec, 1991; Lebioda *et al.*, 1991). As a result, the conformation of these ligands might not fully display a precatalytic complex. On the other hand, the 2-PGA molecule found in the open active site of EhENO is the natural ligand that contains all of the functional groups. While the substrate in subunit *B* very closely resembles the conformation observed for other 2-PGA–enolase complexes in the closed conformation, the 2-PGA molecule in the open active site is shifted slightly away from metal I (Fig. 2*e*). With the exception of Ser40, all active-site residues overlap without major differences. Hence, the 1.3–1.9 Å displacement observed for 2-PGA from the open to the closed state must solely be caused by the closure of L1 and the presence of the second metal ion. Interestingly, the conformation observed in the open active site of EhENO lacks a hydrogen bond between the carboxyl group and metal I and furthermore shows no interaction with Lys398. Together with metal I, Lys398 is believed to stabilize the enolate reaction intermediate (Reed *et al.*, 1996). Notably, the interaction with the acid/base catalysts Glu208/Lys347 can also be observed in the 2-PGA conformation in the open active site. Consequently, the binding of metal II and the closure of L1 fulfil the function of pushing 2-PGA deeper into the active site, which leads to a closer interaction with metal I and Lys398. In order for catalysis to occur, this interaction then stabilizes a carbanion at C_2 of 2-PGA. The importance of L1 closure to catalysis is also supported by the fact that mutations in L1 that substitute Ser40 have a significantly reduced activity in comparison to the wild-type enzyme (Poyner *et al.*, 2002). This could be explained by the notion that closure of L1 protects the reactive carbanion from access to solvent molecules (Wedekind *et al.*, 1994). In summary, the 2-PGA conformation in the open active site of EhENO is most likely to display the precatalytic step of the reaction sequence prior to binding of metal II and closure of L1. This is an important snapshot that provides further insight into a well understood system.

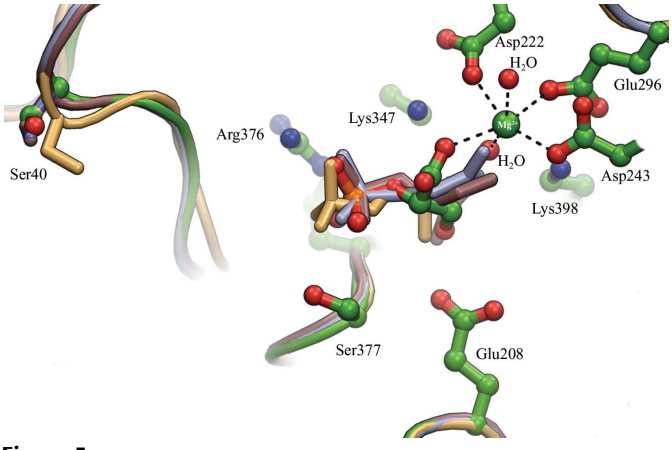

Figure 5
Superposition of enolase structures in the open conformation containing either 2-PGA or phosphoglycolic acid (PGA). Residue numbers are shown for EhENO. While the conformation of 2-PGA in EhENO is more similar to the conformation found in closed active sites, the ligands in other enolase structures differ with respect to the orientation of their carboxyl or hydroxymethyl group. The octahedral coordination of metal I modelled as Mg^{2+} is indicated; waters are shown as red spheres. 3qtp, green (*E. histolytica*); 1pdz, gold (*H. gammarus*); 5enl, purple (*S. cerevisiae*); 6enl, blue (*S. cerevisiae*).

The authors would like to thank Julia Hupfeld for excellent technical assistance and Achim Dickmanns and Piotr Neumann for critical reading of the manuscript. We acknowledge the Helmholtz-Zentrum Berlin electron-storage ring BESSY II for provision of synchrotron radiation at beamline 14.1 and would like to thank Sandra Pühringer for her assistance. This joint research project was financially supported by the State of Lower Saxony and the Volkswagen Foundation, Hannover, Germany.

References

Adams, P. D. *et al.* (2010). *Acta Cryst.* D**66**, 213–221.
Albert, M. A., Haanstra, J. R., Hannaert, V., Van Roy, J., Opperdoes, F. R., Bakker, B. M. & Michels, P. A. (2005). *J. Biol. Chem.* **280**, 28306–28315.
Baxt, L. A. & Singh, U. (2008). *Curr. Opin. Infect. Dis.* **21**, 489–494.
Brewer, J. M. (1981). *CRC Crit. Rev. Biochem.* **11**, 209–254.
Brünger, A. T., Adams, P. D., Clore, G. M., DeLano, W. L., Gros, P., Grosse-Kunstleve, R. W., Jiang, J.-S., Kuszewski, J., Nilges, M., Pannu, N. S., Read, R. J., Rice, L. M., Simonson, T. & Warren, G. L. (1998). *Acta Cryst.* D**54**, 905–921.
Castaldo, C., Vastano, V., Siciliano, R. A., Candela, M., Vici, M., Muscariello, L., Marasco, R. & Sacco, M. (2009). *Microb. Cell Fact.* **8**, 14.
Chai, G., Brewer, J. M., Lovelace, L. L., Aoki, T., Minor, W. & Lebioda, L. (2004). *J. Mol. Biol.* **341**, 1015–1021.
Chang, Y. S., Wu, W., Walsh, G., Hong, W. K. & Mao, L. (2003). *Clin. Cancer Res.* **9**, 3641–3644.
Chen, V. B., Arendall, W. B., Headd, J. J., Keedy, D. A., Immormino, R. M., Kapral, G. J., Murray, L. W., Richardson, J. S. & Richardson, D. C. (2010). *Acta Cryst.* D**66**, 12–21.
da Silva Giotto, M. T., Hannaert, V., Vertommen, D., de A. S. Navarro, M. V., Rider, M. H., Michels, P. A., Garratt, R. C. & Rigden, D. J. (2003). *J. Mol. Biol.* **331**, 653–665.
DeLano, W. L. (2002). *PyMOL*. http://www.pymol.org.
Dokmanić, I., Šikić, M. & Tomić, S. (2008). *Acta Cryst.* D**64**, 257–263.
Duquerroy, S., Camus, C. & Janin, J. (1995). *Biochemistry*, **34**, 12513–12523.
Emsley, P., Lohkamp, B., Scott, W. G. & Cowtan, K. (2010). *Acta Cryst.* D**66**, 486–501.
Esgleas, M., Li, Y., Hancock, M. A., Harel, J., Dubreuil, J. D. & Gottschalk, M. (2008). *Microbiology*, **154**, 2668–2679.
Feo, S., Arcuri, D., Piddini, E., Passantino, R. & Giallongo, A. (2000). *FEBS Lett.* **473**, 47–52.
Hidalgo, M. E., Sánchez, R., Pérez, D. G., Rodríguez, M. A., García, J. & Orozco, E. (1997). *FEMS Microbiol. Lett.* **148**, 123–129.
Hosaka, T., Meguro, T., Yamato, I. & Shirakihara, Y. (2003). *J. Biochem.* **133**, 817–823.
Iida, H. & Yahara, I. (1985). *Nature (London)*, **315**, 688–690.
Kabsch, W. (2010*a*). *Acta Cryst.* D**66**, 125–132.
Kabsch, W. (2010*b*). *Acta Cryst.* D**66**, 133–144.
Kang, H. J., Jung, S.-K., Kim, S. J. & Chung, S. J. (2008). *Acta Cryst.* D**64**, 651–657.
Kim, J. & Dang, C. V. (2005). *Trends Biochem. Sci.* **30**, 142–150.
Kleywegt, G. J. (1996). *Acta Cryst.* D**52**, 842–857.
Kühnel, K. & Luisi, B. F. (2001). *J. Mol. Biol.* **313**, 583–592.
Larsen, T. M., Wedekind, J. E., Rayment, I. & Reed, G. H. (1996). *Biochemistry*, **35**, 4349–4358.
Lebioda, L. & Stec, B. (1988). *Nature (London)*, **333**, 683–686.
Lebioda, L. & Stec, B. (1991). *Biochemistry*, **30**, 2817–2822.

Lebioda, L., Stec, B. & Brewer, J. M. (1989). *J. Biol. Chem.* **264**, 3685–3693.
Lebioda, L., Stec, B., Brewer, J. M. & Tykarska, E. (1991). *Biochemistry*, **30**, 2823–2827.
Martínez, L. I., Piattoni, C. V., Garay, S. A., Rodrígues, D. E., Guerrero, S. A. & Iglesias, A. A. (2011). *Biochimie*, **93**, 260–268.
McCoy, A. J., Grosse-Kunstleve, R. W., Adams, P. D., Winn, M. D., Storoni, L. C. & Read, R. J. (2007). *J. Appl. Cryst.* **40**, 658–674.
McLaughlin, J. & Aley, S. (1985). *J. Protozool.* **32**, 221–240.
Miles, L., Dahlberg, C., Plescia, J., Felez, J., Kato, K. & Plow, E. F. (1991). *Biochemistry*, **30**, 1682–1691.
Navarro, M. V. D. A. S., Gomes Dias, S. M., Mello, L. V., Da Silva Giotto, M. T., Gavalda, S., Blonski, C., Garratt, R. C. & Rigden, D. J. (2007). *FEBS J.* **274**, 5077–5089.
Nurmohamed, S., McKay, A. R., Robinson, C. V. & Luisi, B. F. (2010). *Acta Cryst.* D**66**, 1036–1040.
Pancholi, V. (2001). *Cell. Mol. Life Sci.* **58**, 902–920.
Petri, W. A. (2003). *Trends Parasitol.* **19**, 523–526.
Poyner, R. R., Cleland, W. W. & Reed, G. H. (2001). *Biochemistry*, **40**, 8009–8017.
Poyner, R. R., Larsen, T. M., Wong, S.-W. & Reed, G. H. (2002). *Arch. Biochem. Biophys.* **401**, 155–163.
Py, B., Higgins, C. F., Krisch, H. M. & Carpousis, A. J. (1996). *Nature (London)*, **381**, 169–172.
Reed, G. H., Poyner, R. R., Larsen, T. M., Wedekind, J. E. & Rayment, I. (1996). *Curr. Opin. Struct. Biol.* **6**, 736–743.
Reeves, R. E. (1984). *Adv. Parasitol.* **23**, 105–142.
Reyes-Vivas, H., Diaz, A., Peon, J., Mendoza-Hernandez, G., Hernandez-Alcantara, G., De la Mora-De la Mora, I., Enriquez-Flores, S., Dominguez-Ramirez, L. & Lopez-Velazquez, G. (2007). *J. Mol. Biol.* **365**, 752–763.
Rosenbaum, R. M. & Wittner, M. (1970). *J. Cell Biol.* **45**, 367–382.
Samarawickrema, N. A., Brown, D. M., Upcroft, J. A., Thammapalerd, N. & Upcroft, P. (1997). *J. Antimicrob. Chemother.* **40**, 833–840.
Segovia-Gamboa, N. C., Chávez-Munguía, B., Medina-Flores, Y., Cázares-Raga, F. E., Hernández-Ramírez, V. I., Martínez-Palomo, A. & Talamás-Rohana, P. (2010). *Exp. Parasitol.* **125**, 63–69.
Sims, P. A., Menefee, A. L., Larsen, T. M., Mansoorabadi, S. O. & Reed, G. H. (2006). *J. Mol. Biol.* **355**, 422–431.
Stec, B. & Lebioda, L. (1990). *J. Mol. Biol.* **211**, 235–248.
Subramanian, A. & Miller, D. M. (2000). *J. Biol. Chem.* **275**, 5958–5965.
Tally, F. P., Sutter, V. L. & Finegold, S. M. (1975). *Antimicrob. Agents Chemother.* **7**, 672–675.
Tovy, A., Siman Tov, R., Gaentzsch, R., Helm, M. & Ankri, S. (2010). *PLoS Pathog.* **6**, e1000775.
Wedekind, J. E., Poyner, R. R., Reed, G. H. & Rayment, I. (1994). *Biochemistry*, **33**, 9333–9342.
Wedekind, J. E., Reed, G. H. & Rayment, I. (1995). *Biochemistry*, **34**, 4325–4330.
World Health Organization (1997). *Bull. World Health Organ.* **75**, 291–294.
Wistow, G. & Piatigorsky, J. (1987). *Science*, **236**, 1554–1556.
Zhang, E., Brewer, J. M., Minor, W., Carreira, L. A. & Lebioda, L. (1997). *Biochemistry*, **36**, 12526–12534.